FUDMA Journal of Sciences (FJS)
ISSN online: 2616-1370
ISSN print: 2645 - 2944
Vol. 10 No. 12, June, 2026, pp 325 – 332
DOI: https://doi.org/10.33003/fjs-2026-1012-5629

Effect of Rhenium Doping on Basal Plane Activation of 1H-WX_2 (X = S, Se, Te) Electrocatalysts for Improved Hydrogen Evolution Reaction: A First-Principles Study

Shamsuddeen Sani Alhassan, Mahmud Abdulsalam, Abdullahi Tanimu and *Muhammad Ibrahim Bagudo

Department of Physics, Umaru Musa Yar'adua University, Katsina State, Nigeria.

*Corresponding authors' email: ibrahim.bagudo@umyu.edu.ng

Received: 20th July 2026
Accepted: 23rd July 2026
Published: 5th August 2026

ABSTRACT
The development of earth-abundant and low-cost electrocatalysts for hydrogen evolution reaction (HER) is essential for sustainable hydrogen production through water electrolysis. In this work, density functional theory (DFT) calculations were employed to systematically investigate how substitutional rhenium (Re) doping activates the basal plane of pure 1H-WX_2 (X = S, Se, Te) monolayers. Two doping concentrations, namely 25% and 50%, were considered to elucidate the concentration-dependent catalytic behavior. Our results revealed that the hexagonal crystal symmetry of the host lattice is preserved after Re substitution, and negative dopant formation energies across all 25% doping systems establish their thermodynamic stability while the 50% Re doping systems were thermodynamically unstable due to positive formation energies. Hydrogen adsorption analysis demonstrated that pristine WX_2 monolayers possess weak catalytic activity due to unfavorable hydrogen adsorption free energy (ΔG_{H^*}). However, Re doping significantly improved HER performance. Among all investigated systems, the 25% Re-doped WS_2 monolayer ($W_{0.75}Re_{0.25}S_2$) exhibited the most favorable HER activity with a ΔG_{H^*} value of -0.16 eV. Volcano plot analysis further established that moderate Re doping (25%) provides the optimal catalytic performance, whereas excessive doping (50%) leads to hydrogen over-binding. Density of states analysis showed that Re incorporation induces semiconductor-to-metal transitions in all WX_2 systems through the introduction of impurity states near the Fermi level, which may facilitates charge-transfer kinetics during catalysis. This study demonstrates that Re doping is an effective strategy for tuning the catalytic activity of tungsten dichalcogenides and highlights Re-doped WX_2 monolayers, particularly $W_{0.75}Re_{0.25}S_2$, as promising non-precious electrocatalyst for efficient hydrogen production.

Keywords: Rhenium; Doping; Density functional theory; Tungsten dichalcogenides; Hydrogen evolution reaction; Volcano plot; Electrocatalysts

INTRODUCTION

The increasing global demand for clean and sustainable energy has driven intensive research into green hydrogen production via water splitting. This process involves two basic half-reactions: the hydrogen evolution reaction (HER) at the cathode and the oxygen evolution reaction (OER) at the anode (Fu et al., 2020). While precious platinum group materials exhibit excellent HER performance, their scarcity and high cost severely limit large-scale industrial adoption (Stamenkovic et al., 2017; Zhu et al., 2020). Consequently, developing cost-effective, earth-abundant, and highly efficient electrocatalysts has become a central goal in the field.

In this context, two-dimentional (2D) transition metal dichalcogenides (TMDs) have emerged as promising alternatives due to their unique and excellent structural and electronic properties especially the molybdenum (Mo) and tungsten (W)-based dichalcogenides with general formula MX_2 (M=Mo, W; X=S, Se, Te) (Alhassan et al., 2025; Sukanya et al., 2022). Compared to Mo, W is more earth-abundant and its derivatives are more environmentally friendly (Huang et al., 2022). However, WX_2 (X=S, Se, Te) materials exist in multiple phases that span semiconducting (2H/1H), metallic (1T), and distorted (1T′) structures-offering versatile platforms for catalytic applications (Huang et al., 2020; Ye et al., 2018). Despite these advantages, pure WX_2 materials face one critical problem which is the non-reactivity of their basal planes-resulting in lower catalytic performance compared to Platinum-based materials (Jaramillo et al., 2007). To overcome this challenge, various strategies have been explored, including defect engineering, phase modulation, heterostructures (Alhassan et al., 2025; Sukanya et al., 2022; Vikraman et al., 2021). Among these, defect engineering particularly substitutional doping (especially with transition metals) has emerged as a highly effective approach to activate inert basal planes and optimize electronic structures (Zhang et al., 2020).

Extensive studies have demonstrated that both transition metal and non-metal dopants can significantly enhance the HER activity of WX_2 systems. For example, Fe-doped WS_2 monolayer exhibits a reduced overpotential of 195 mV in comparison to its pure counterpart (Kang et al., 2021). Zhang et al. (2021) reported that Cobalt doping in WSe_2 has demonstrated a significant improvement in the HER performance compared to the pristine WSe_2 (Zhang et al. (2021). Similarly, comparative investigations involving five different transition metals (Fe, Co, Nb, Ni, and Zr) dopants revealed that Ni-doped WSe_2 delivers superior HER activity (Kadam et al., 2020). In addition, light-elements doping (such as B, N, P, and O) has been shown to enhance conductivity and optimize hydrogen adsorption behavior in WX_2 systems (Huang et al., 2022; Sarma et al., 2020; Sun et al., 2022; Wang

et al., 2020; Wang et al., 2022). Despite these advances, the catalytic performance of doped WX_2 still lags behind that of precious platinum group, highlighting the need for alternative dopants with more favorable electronic interactions.

To this effect, experimental and theoretical studies suggest that substitutional doping of group VI TMDs (MX_2, where M = Mo, W and X = S, Se) with elements from Groups V-VII is energetically favorable, particularly at metal sites rather than interstitial or defect positions (Dolui et al., 2013; Lin et al., 2014). Among these, rhenium (Re) stands out as a particularly promising dopant due to its comparable atomic radius to tungsten and molybdenum (1.37 Å for Re vs. 1.39 Å for W and 1.39 Å for Mo), which minimizes lattice distortion upon substitution and its excellent intrinsic catalytic activity (Luo & Liang, 2024). Previous reports have shown that Re incorporation can increase the density of active sites, introduce n-type doping, induce phase transitions (e.g., from 2H to metallic 1T phases), and enhance catalytic as well as electro-chemical performances in MoS_2-based materials (Aliaga et al., 2019; Chhetri et al., 2015; Sigiro et al., 2015; Woo et al., 2015). However, Re-doped WS_2 nanotubes were revealed to have demonstrated higher strain than the parent material (2H-WS_2 nanotube) (Enyashin et al., 2011).

To the best of our knowledge, despite all these promising attributes, doping the complete WX_2 (X=S, Se, Te) family with Re for HER applications has not been systematically explored. Most of the existing works focused only on MoS_2 systems, leaving a gap in understanding the catalytic capability of the Re-doped 1H-WX_2 (X=S, Se, T e) materials. Therefore, in this work, we address this gap by performing a comprehensive density functional theory (DFT) investigation on Re-doped WX_2 (X = S, Se, Te) monolayers. Specifically, we examine how varying Re concentrations (25% and 50%) influence the structural stability, electronic properties, and catalytic performance of these materials. By systematically comparing sulfide, selenide, and telluride systems, this study provides new insights into the interplay between dopant concentration, chalcogen chemistry, and catalytic activity.

MATERIALS AND METHODS

All density functional theory (DFT) calculations were performed using Quantum ESPRESSO simulation package (Giannozzi et al., 2009). A 2x2x1 supercells of the 1H-WX_2 (X = S, Se, Te) monolayers were used as the starting model. To account for van der Waals (vdW) interactions, the DFT-D3 correction scheme was employed (Grimme et al., 2010). The exchange-correlation potential was described using the generalized gradient approximation (GGA) in the Perdew-Burke-Ernzerhof (PBE) parameterization (Perdew et al., 1996). Since standard GGA typically underestimates bandgaps, a DFT+U (Hubbard on-site correction) approach was adopted, with an effective U value of 5 eV applied to both W and Re atoms. This value was chosen because it reproduces experimental bandgaps for the pure systems (Creazzo, 2025). The electron-ion core interaction was treated with ultrasoft pseudopotentials, explicitly including the following valence orbitals: W ($5d^4\ 6s^2$), Re ($5d^5\ 6s^2$), S ($3s^2\ 3p^4$), Se ($4s^2\ 4p^4$), Te ($5s^2\ 5p^4$), and H ($1s^1$). A plane-wave kinetic energy cutoff of 612 eV was used for all calculations. Brillouin-zone integration was carried out using Monkhorst-Pack sampling with an 8×8×1 k-point grid. A vacuum layer of 20 Å was added along the c-direction (perpendicular to the monolayer) to prevent spurious interactions between periodic images. Full structural relaxation was performed using the Broyden-Fletcher-Goldfarb-Shanno (BFGS) algorithm.

For the doping models, two different doping concentrations were considered-25% and 50% Re doping. The 25% Re doping was constructed by removing one W atom and replacing with a Re atom, yielding $W_{0.75}Re_{0.25}X_2$(X= S, Se, Te). Whereas the 50% Re doing was achieved by substituting two W atoms with other two Re atoms, giving $W_{0.5}Re_{0.5}X_2$(X= S, Se, Te).

RESULTS AND DISCUSSION

Structural Properties of Pure and Re-Doped WX_2(X=S, Se, Te) Monolayers

The initial crystal parameters for the bulk WX_2 (S, Se, Te) materials were obtained from material project database (Jain et al., 2013). The 1H-WX_2 (S, Se, Te) monolayers constructed exhibit a hexagonal crystal structure with space group $P6_3/mmc$. The optimized lattice constant a for the different monolayers was displayed in Table 1. Our calculated lattice constants for the pure materials show excellent agreement with previously reported theoretical and experimental values (Schutte et al., 1987; Vuong et al., 2018), validating our computational method. However, the hexagonal structure was preserved even after the Re substitution as shown in Figure 1, demonstrating that the host lattice can accommodate substantial Re incorporation without much structural collapse. The lattice parameter (a) decreases systematically with increasing Re concentration for all three dichalcogenides (Table 1). For WS_2, the lattice constant contracts by 7.0% and 9.6%, for 25% and 50% Re doping respectively. Similar reduction trends are observed for WSe_2 (7.4% and 10.7%) and WTe_2 (7.4% and 11.0%). This contraction reflects the slightly smaller atomic radius of Re atom and the formation of stronger Re-X bonds compared to W-X bonds, which may lead to enhanced metal-chalcogen covalency. Also, the unit-cell volume decreases monotonically across all the doped materials as shown in Table 1.

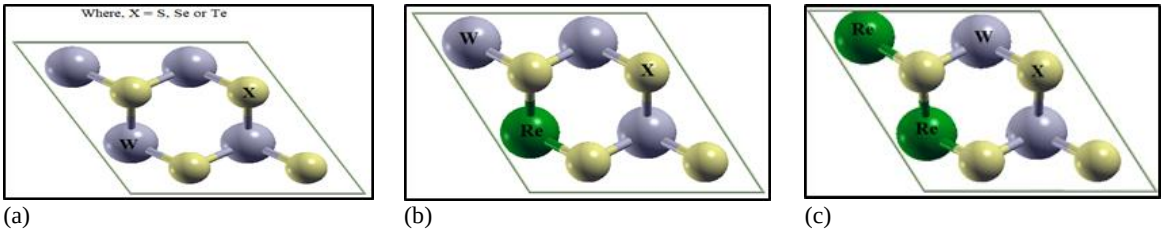

(a) (b) (c)

Figure 1: Optimized crystal structures of: (a) Pure 1H-WX_2 (X=S, Se, Te) (b) 25% Re-doped 1H-WX_2 (X=S, Se, Te) and (c) 50% Re-doped 1H-WX_2 (X=S, Se, Te) monolayers

Table 1: Lattice Parameter (a) for the Pure and Doped Materials, Tungsten-Chalcogen (W-X) and Rhenium-Chalcogen (Re-X) Bond Lengths, Unit Cell Volumes (V_{cell}) and Dopant Formation Energies (E_f) of the Doped Systems

S/N	Materials	(a) (Å)	W-X (Å)	Re-X (Å)	E_f (eV)	V_{Cell} (Å^3)
1	Pure WS_2	3.1896	2.4195	-	-	1538.9388
2	$W_{0.75}Re_{0.25}S_2$	2.9659	-	2.3921	-2.7069	1330.6959
3	$W_{0.5}Re_{0.5}S_2$	2.8838	-	2.4140	3.7913	1259.7176
4	Pure WSe_2	3.3226	2.5520	-	-	1685.2910
5	$W_{0.75}Re_{0.25}Se_2$	3.0779	-	2.5235	-3.1399	1446.5029
6	$W_{0.5}Re_{0.5}Se_2$	2.9672	-	2.5299	3.6844	1339.5355
7	Pure WTe_2	3.5560	2.7479	-	-	1959.3257
8	$W_{0.75}Re_{0.25}Te_2$	3.2919	-	2.6821	-3.7635	1676.3585
9	$W_{0.5}Re_{0.5}Te_2$	3.1645	-	2.6933	2.6236	1551.5160

To assess the thermodynamic stability of the doped structures, dopant formation energies were computed according to equation (1) (Alhassan & Abdulsalam, 2024; Dorian et al., 2012), and the results were displayed in Table 1.

$$E_f = E_{doped} + E_{pure} + \mu_W - \mu_{\Re}. \quad (1)$$

Where E_{doped} and E_{pure} are the DFT total energies of the doped and pure systems, μ_W and $\mu_{\Re}$ are chemical potentials (total energy per atom) of bulk W and bulk Re crystals, respectively.

The calculated E_f values are negative for all 25% Re-doped systems, confirming that substitutional Re doping is thermodynamically feasible and favorable in the materials. Whereas the 50% Re-doped systems exhibited positive dopant formation energies revealing their thermodynamically instability. The increasingly negative values from S – Te (in the 25% doping level) suggest that Re incorporation becomes more favorable with increasing chalcogen atomic size. On the other hand, the decreasing positive values associated to 50% Re doping (from S – Te) signifies less instability in the selenide and telluride compared to the sulfide. That is to say, even for the 50% doping model, the heavier chalcogens were less unstable.

Hydrogen Adsorption and HER activity

The process of electrocatalytic water splitting is facilitated through two main half reactions which normally takes place at two different electrodes of an electrolyzer. HER at the cathode and OER at the anode. The HER is the main reaction that leads to the evolution of hydrogen. In acidic electrolytes, it proceeds through two primary mechanisms: Volmer-Tafel (equations 2 and 3) or Volmer-Heyrovsky (equation 4). The hydrogen adsorption site is represented by the symbol "*" in this description (Fu et al., 2020).

$$* + H^+ + e^- \rightarrow H^*_{ads} \quad (2)$$

$$2H^*_{ads} \rightarrow H_2 + 2^*. \quad (3)$$

$$* + H^+ + e^- + H^*_{ads} \rightarrow H_2 + *. \quad (4)$$

Hydrogen adsorption step is common to both mechanisms and very important. The strength of this adsorption is quantified by the Gibbs free energy change, (ΔG_{H^*}), a crucial descriptor for HER performance and is calculated according to equations (5) or (7) (Huang et al., 2022; Ogunkunle et al., 2024)

$$\Delta G_H = \Delta E_H - T\Delta S + \Delta E_{ZPE}. \quad (5)$$

$$\Delta E_H = E_H - E - \frac{1}{2}E_{H_2}. \quad (6)$$

Where, E_{H^*} and E^* are the energies of the WX_2 (X= S, Se, Te) monolayers with and without adsorbed H atoms, respectively, E_{H2} is the energy of the free H_2 molecule, T is the room temperature (T=298.15 K), ΔS is the entropy change, and ΔZPE is the zero-point energy change.

However, equation (5) can be written as (Nørskov et al., 2005):

$$\Delta G_H = \Delta E_H + 0.24. \quad (7)$$

Three different adsorption sites for the H on the surface of the electrocatalysts were considered. This is because the value of adsorption energy varies with positions. The sites are (I) on top of W, (II) on top of X, and (III) a bridge. At each position, the adsorption energy was calculated using equation (6), and the results were shown in Figure 2. Based on the result, H preferred to be adsorbed in between the W and X (bridge) for the cases of pure WS_2 and WSe_2 monolayers, whereas adsorption on top of W is the most stable for the WTe_2 monolayer.

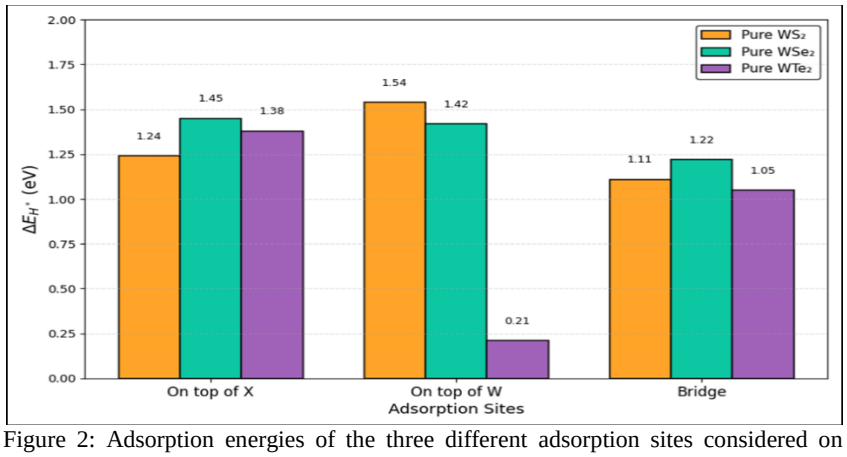

Figure 2: Adsorption energies of the three different adsorption sites considered on surface of the pure 1H-WX_2 (S, Se, Te) monolayers

To explore the catalytic performance of the 1H-WX_2 (S, Se, Te) monolayers for HER process, the ΔG_{H^*} for the most stable adsorption sites was calculated according to equation (7); the results are depicted in Figure 3. An ideal electrocatalyst exhibits ΔG_{H^*} close to zero, indicating optimal hydrogen binding neither too weak nor too strong (Nørskov et al., 2005). The pure WX_2 monolayers display strongly positive ΔG_{H^*} values particularly the WS_2 and WSe_2, confirming their intrinsically poor HER activity due to weak hydrogen adsorption on the inert basal plane.

Moreover, Re doping dramatically enhances hydrogen adsorption as seen from Figure 3. For WS_2, ΔG_{H^*} decreases from 1.35 eV to -0.16 eV at 25% Re substitution, placing it remarkably close to the optimal zero value. However, the near-zero adsorption free energy signifies that Re may effectively activates the basal plane of the pure system. A similar, though less pronounced, improvement is observed for WSe_2 at the same concentration level. Re substitution lowers ΔG_{H^*} substantially, indicating stronger hydrogen binding and possible enhancement in the catalytic activity. On the other hand, at higher Re concentrations (50%), however, hydrogen adsorption becomes excessively strong, yielding highly negative ΔG_{H^*} values. For example, $W_{0.5}Re_{0.5}S_2$ exhibits ΔG_{H^*} = -1.41 eV. Such overbinding can impede hydrogen desorption and thus reduce HER turnover.

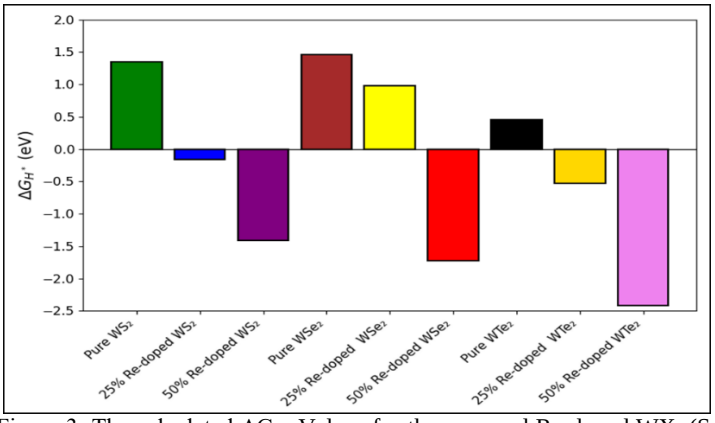

Figure 3: The calculated ΔG_H. Values for the pure and Re-doped WX_2 (S, Se, Te) materials

However, according to our results, the low Re-doping (25%) on the 1H-WX_2 (S, Se, Te) monolayers gives the most favorable ΔG_{H^*} values, particularly $W_{0.75}Re_{0.2}S_2$-exhibits the most favorable HER thermodynamics among the studied materials. Similar trend was observed experimentally in Re-doped MoS_2, where low Re-doping reduces charge-transfer resistance in the material and enhances its catalytic activity (in HER) better than the higher concentration levels (Aliaga et al., 2019).

Theoretical Exchange Current Density and Volcano Plot

The theoretical exchange current density (i_0) represents the rate of the proton transfer to the surface, which can be derived on the basis of ΔG_{H^*}. At standard conditions (pH = 0 and T = 300 K), the i_0 can be computed using equations (8) and (9) when the proton transfer is exothermic (ΔG_H < 0) and endothermic (ΔG_H > 0) respectively (Nørskov et al., 2005).

$$i_0 = \frac{-ek_0}{1+exp\left(\frac{-\Delta G}{KT}_H\right)} \quad (8)$$

$$i_0 = \frac{-ek_0 exp\left(\frac{-\Delta G}{KT}_H\right)}{1+exp\left(\frac{-\Delta G}{KT}_H\right)}. \quad (9)$$

Where, k_0 is the rate constant (200 s^{-1}/site) and K is the Boltzmann constant.

However, improved electrocatalytic activity and quicker reaction kinetics are indicated by a larger exchange current density. Catalysts with ΔG_{H^*} values closest to zero exhibit the highest intrinsic HER activity. Consequently, $W_{0.75}Re_{0.25}S_2$ is expected to deliver the largest exchange current density among all studied systems. Its location near the apex of the HER volcano plot confirms its optimal hydrogen-binding strength as depicted in Figure 4.

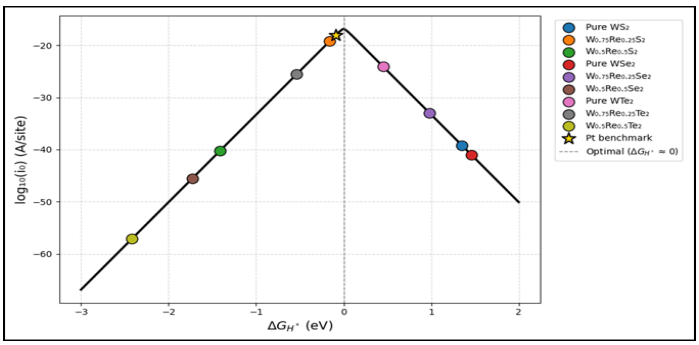

Figure 4: Volcano plot constructed using the Gibbs free energy of hydrogen adsorption (ΔG_{H^*}) and theoretical exchange current density (i_0) for pure and Re-doped WX_2 (X = S, Se, Te) monolayers, with Pt (111) included as a reference catalyst

In contrast, pure WX_2 materials lie on the weak-binding branch of the volcano (right side), where sluggish proton adsorption limits activity. The 50% Re-doped systems shift to the strong-binding branch (left side), where hydrogen desorption becomes rate-limiting. The volcano plot therefore clearly also identifies moderate Re doping as the optimal strategy for maximizing catalytic performance.

Electronic Properties

The electronic origin of the enhancement observed in the catalytic performance of the doped systems is explained based on analysis of the density of states and differential charge densities of the pure and doped materials.

Density of States (DOS)

The density of states (DOS) of the pure and doped systems were plotted (Figures 5a-5i) to further elucidate the electronic origin of the improvement observed in the catalytic performance of the doped materials. It is important to understand that the electronic states near the Fermi level play a crucial role in governing charge-transfer kinetics and catalytic efficiency of materials (Deng et al., 2019; Meng et al., 2018). Figures 5a, 5d, and 5g show the DOS plots for the pure 1H-WX_2 (X=S, Se, Te) monolayers. They all exhibit a semiconducting behavior as evidenced from their bandgaps, 1.9 eV, 1.7 eV, and 1.2 eV for WS_2, WSe_2, and WTe_2 monolayers, respectively. These values are in reasonable agreement with previously reported data (Creazzo, 2025; Do et al., 2019; Kumar & Ahluwalia, 2012; Tonndorf et al., 2013). However, it can be seen that the valence bands of the pure systems are largely populated by most of the states, leaving the corresponding conduction bands with minor states.

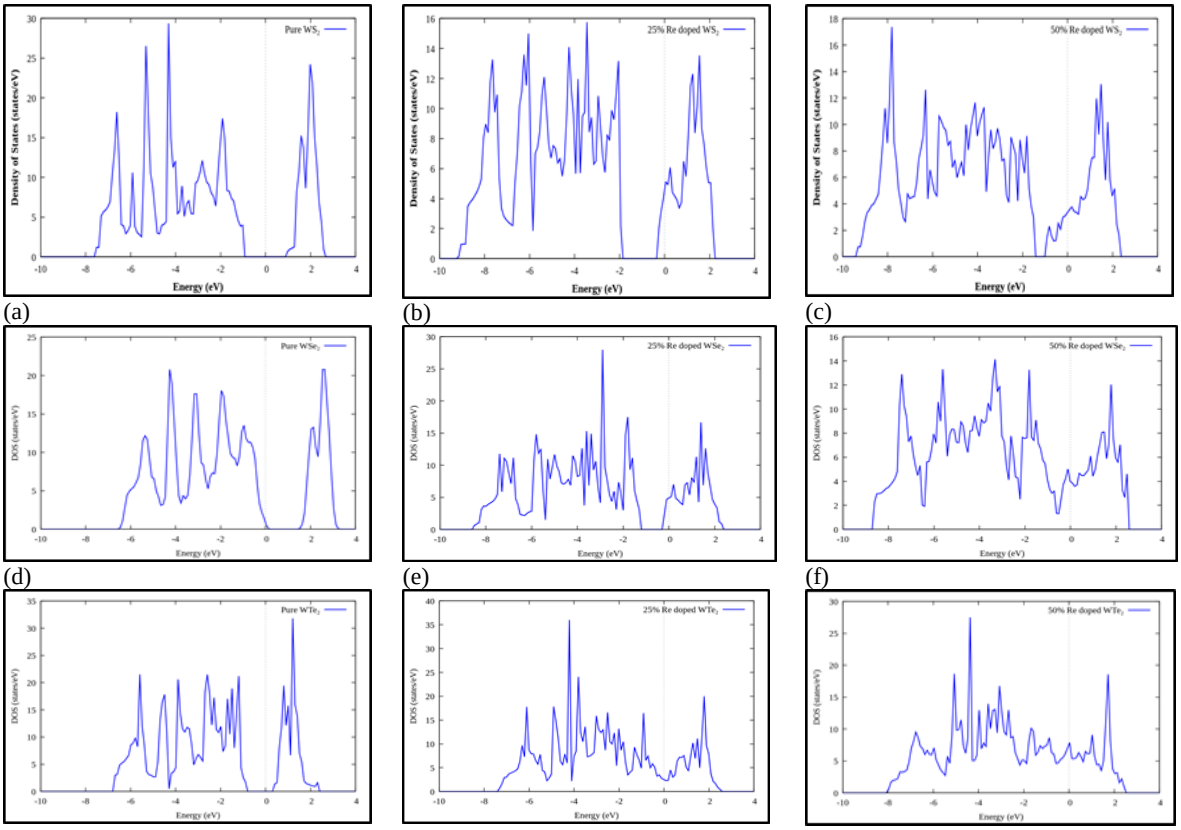

Figure 5: Density of states for: (a) Pure WS_2 (b) 25% Re-doped WS_2 (c) 50% Re-doped WS_2 (d) Pure WSe_2 (e) 25% Re-doped WSe_2 (f) 50% Re-doped WSe_2 (g) Pure WTe_2 (h) 25% Re-doped WTe_2 (i) 50% Re-doped WTe_2. The Fermi level is set at 0.0 eV.

The electronic structures of 1H-WX_2 (X=S, Se, Te) were profoundly changed after Re doping. However, additional states were emerged near the Fermi level, leading to complete metallization of the doped systems. This transition may be originated from the additional valence electron contributed by Re relative to W. As a result, Re behaves as an n-type dopant, shifting the Fermi level upward into the conduction band for all the doped systems (Figures 5b, 5c, 5e, 5f, 5h, 5i). The increased electronic states near the Fermi level may enhance carrier concentration and electrical conductivity-two critical parameters for electrocatalytic performance of a material. Additionally, while high conductivity is beneficial, catalytic activity depends critically on achieving an optimal balance between electron transport and hydrogen-binding strength.

Charge Density Difference (CDD)

The charge redistribution that exists through bonding interaction between the adsorbed H and the surface of the electrocatalysts is explained using charge density difference ($\Delta\rho$). It is defined by the following relation (Huang et al., 2022):

$$\Delta\rho = \rho_{catalyst+H} - \rho_{catalyst} - \rho_H \quad (10)$$

Where, $\rho_{catalyst+H}$, $\rho_{catalyst}$ and ρ_H are charge densities of catalyst with adsorbed H, catalyst without adsorbed H and isolated H atom respectively.

The charge density difference (CDD) plots in Figure 6 show the electronic interaction between the adsorbed hydrogen and the pure and Re-doped WX_2 (X = S, Se, Te) monolayers. The yellow and blue regions represent charge accumulation and

depletion, respectively, indicating electron redistribution during adsorption.

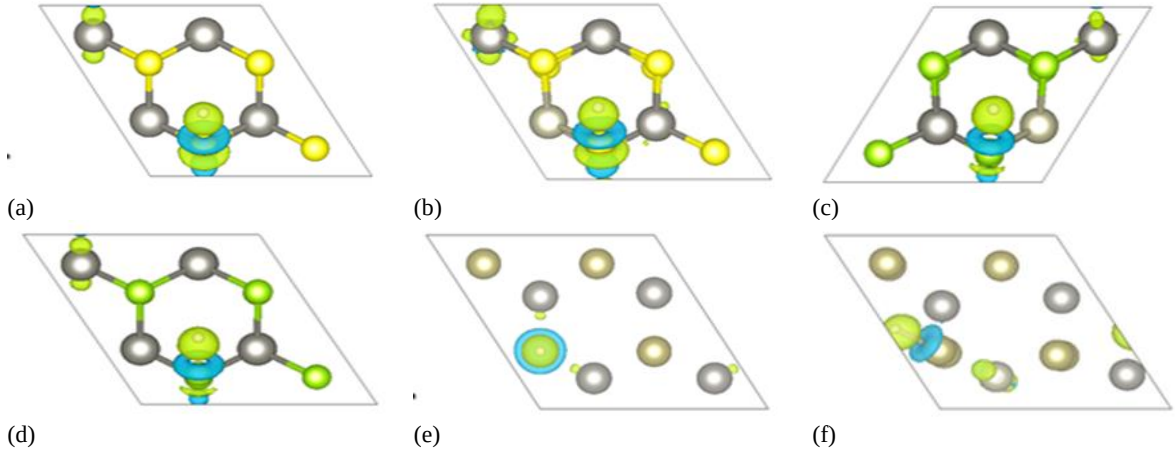

Figure 6: Charge density differences of: (a) Pure WS_2 (b) Re-doped WS_2 (c) Pure WSe_2 (d) Re-doped WSe_2 (e) Pure WTe_2 (f) Re-doped WTe_2. The isosurface value used is 0.007 e/ Å. The yellow and blue colors represent charge accumulation and depletion respectively

For the pure WS_2, WSe_2 and WTe_2 systems, charge redistribution is relatively localized around the adsorption site, suggesting moderate interaction between adsorbed hydrogen and the surface of the catalyst. The charge accumulation seen around the adsorbed H for all the systems signifies a charge transfer from the catalyst to the adsorbate similar to what was reported for 1T'-WX_2 (Huang et al., 2022). Furthermore, it is observed that WTe_2 exhibits a more diffuse charge distribution among the studied systems, which may be attributed to the larger atomic size and lower electronegativity of Te atoms compared to S and Se atoms.
However, after Re doping, the charge accumulation around the adsorption region becomes significantly stronger and more delocalized for all systems. This improved redistribution indicates increased electron transfer and stronger orbital hybridization between the adsorbed hydrogen and the surface of the catalyst. Additionally, this suggests improved electrical conductivity and optimized adsorption behavior, both of which are essential for efficient hydrogen evolution reaction (HER) activity.

CONCLUSION

In this work, first-principles DFT calculations were performed to investigate the effects of substitutional Re doping on the basal plane activation of 1H-WX_2 (X = S, Se, Te) monolayers. The calculated negative formation energies for the 25% doping and positive formation energies for the 50% doping concentration confirmed that Re incorporation into the WX_2 lattice is thermodynamically favorable and unfavorable respectively for the two different doping levels. Hydrogen adsorption calculations revealed that pristine WX_2 monolayers exhibit poor HER performance because of weak hydrogen adsorption on the inert basal plane. Remarkably, Re substitution substantially improved the catalytic activity by tuning the hydrogen adsorption free energy toward the thermoneutral region. Among all investigated systems, the 25% Re-doped WS_2 monolayer demonstrated the best catalytic performance with a ΔG_{H^*} value very close to zero, suggesting optimal adsorption/desorption kinetics for HER. In contrast, excessive Re incorporation at 50% concentration resulted in overly strong hydrogen binding, which may hinder hydrogen desorption and reduce catalytic turnover. Electronic structure analysis demonstrated that Re doping induces significant metallization of the WX_2 monolayers through the emergence of impurity states near the Fermi level. Charge density difference analysis further confirmed stronger orbital hybridization and enhanced electron redistribution between adsorbed hydrogen and the catalyst surface after Re doping. These effects collectively explain the improved HER activity observed in the doped systems. Taken together, these findings carry direct practical significance for the design of next-generation HER electrocatalysts: because Re and WX_2 are far more earth-abundant and less costly than platinum-group metals, and because the 25% doping level identified here is possibly dilute enough to be experimentally accessible via established chemical vapor deposition or solid-state doping routes. This work establishes substitutional Re doping as an effective electronic structure engineering strategy for activating inert basal planes of tungsten dichalcogenides toward efficient hydrogen evolution. The findings provide valuable theoretical insights for the rational design of high-performance and earth-abundant HER electrocatalysts and identify $W_{0.75}Re_{0.25}S_2$ as a particularly promising candidate for sustainable hydrogen production applications. We recommend future experimental validation, such as electrochemical testing of Re-doped WS_2 thin films, to confirm the predicted catalytic gains.

REFERENCES

Alhassan, S. S. & Abdulsalam, M. (2024). A DFT+U study of the structural and electronic properties of zinc-doped anatase TiO_2 nanomaterial. UMYU Scientifica, 3(1), 186–191. https://doi.org/10.56919/usci.2431.020

Alhassan, S. S., Abdulsalam, M., & Tanimu, A. (2025). Application of transition metals dichalcogenides in electrocatalytic splitting of water for hydrogen production: A review. Nigerian Journal of Physics, 34(2), 44. https://doi.org/10.62292/njp.v34i2.2025.366

Aliaga, J., Vera, P., Araya, J., Ballesteros, L., Urzúa, J., Farías, M., Paraguay-Delgado, F., Alonso-Núñez, G., González, G., & Benavente, E. (2019). Electrochemical hydrogen evolution over hydrothermally synthesized Re-doped MoS_2 flower-like microspheres. Molecules, 24(24), 4631. https://doi.org/10.3390/molecules24244631

Chhetri, M., Gupta, U., Yadgarov, L., Rosentsveig, R., Tenne, R., & Rao, C. N. R. (2015). Beneficial effect of Re doping on the electrochemical HER activity of MoS2 fullerenes. Dalton Transactions, 44(37), 16399–16404.

Creazzo, F. (2025). Engineering of $MoSe_2$ and WSe_2 monolayers and heterostructures by DFT-molecular dynamics simulations. ACS Applied Materials & Interfaces, 17, 39676–39693.

Deng, C., He, R., Shen, W., Li, M., & Zhang, T. (2019). A single-atom catalyst of cobalt supported on a defective two-dimensional boron nitride material as a promising electrocatalyst for the oxygen reduction reaction: A DFT study. Physical Chemistry Chemical Physics, 21(13), 6900–6907. https://doi.org/10.1039/C9CP00452A

Do, M., Nguyen, N. H., Phung, H. T. T., Phuc, H. V., Amin, B., Hoi, B. D., Hieu, N. V., Nhan, L. C., Nguyen, C. V., & Le, P. T. T. (2019). Electronic properties of WS_2 & WSe_2 monolayers with biaxial strain: A first principle study. Chemical Physics, 519, 69–73.

Dolui, K., Rungger, I., Das Pemmaraju, C., & Sanvito, S. (2013). Origin of the n-type and p-type conductivity of MoS_2 monolayers on a SiO_2 substrate. Physical Review B, 88, 075420.

Dorian, A. H. H., Mohammed, H. N. A., Sean, L., Aibing, Y., & Charles, C. S. (2012). Ab initio study of phase stability in doped TiO_2. Computational Mechanics, 50(2), 185–194.

Enyashin, A. N., Yadgarov, L., Houben, L., Popov, I., Weidenbach, M., Tenne, R., Bar-Sadan, M., & Seifert, G. (2011). New route for stabilization of 1T-WS_2 and MoS_2 phases. The Journal of Physical Chemistry C, 115(50), 24586–24591.

Fu, Q., Han, J., Wang, X., Xu, P., Yao, T., Zhong, J., Zhong, W., Liu, S., Gao, T., Zhang, Z., Xu, L., & Song, B. (2020). 2D transition metal dichalcogenides: Design, modulation, and challenges in electrocatalysis. Advanced Materials, 32, 1907818. https://doi.org/10.1002/adma.201907818

Giannozzi, P., Baroni, S., Bonini, N., Calandra, M., Car, R., Cavazzoni, C., Ceresoli, D., Chiarotti, G. L., Cococcioni, M., Dabo, I., Dal Corso, A., Fabris, S., Fratesi, G., de Gironcoli, S., Gebauer, R., Gerstmann, U., Gougoussis, C., Kokalj, A., Lazzeri, M., Wentzcovitch, R. M. (2009). QUANTUM ESPRESSO: A modular and open-source software project for quantum simulations of materials. Journal of Physics: Condensed Matter, 21(39), 395502. https://doi.org/10.1088/0953-8984/21/39/395502

Grimme, S., Antony, J., Ehrlich, S., & Krieg, H. (2010). A consistent and accurate ab initio parametrization of density functional dispersion correction (DFT-D) for the 94 elements H-Pu. The Journal of Chemical Physics, 132, 154104. https://doi.org/10.1063/1.3382344

Huang, H., Fan, X., Singh, D. J., & Zheng, W. (2020). Recent progress of TMD nanomaterials: Phase transitions and applications. Nanoscale, 12(3), 1247–1268.

Huang, H., Hu, G., Hu, C., & Fan, X. (2022). Enhanced hydrogen evolution reactivity of T′-phase tungsten dichalcogenides (WS_2, WSe_2, and WTe_2) materials: A DFT study. International Journal of Molecular Sciences, 23(19), 11727. https://doi.org/10.3390/ijms231911727

Jain, A., Ong, S. P., Hautier, G., Chen, W., Richards, W. D., Dacek, S., Cholia, S., Gunter, D., Skinner, D., Ceder, G., & Persson, K. A. (2013). The Materials Project: A materials genome approach to accelerating materials innovation. APL Materials, 1(1), 011002. https://doi.org/10.1063/1.4812323

Jaramillo, T. F., Jørgensen, K. P., Bonde, J., Nielsen, J. H., Horch, S., & Chorkendorff, I. (2007). Identification of active edge sites for electrochemical H2 evolution from MoS2 nanocatalysts. Science, 317(5834), 100–102. https://doi.org/10.1126/science.1141483

Kadam, S. R., Enyashin, A. N., Houben, L., Bar-Ziv, R., & Bar-Sadan, M. (2020). Ni–WSe2 nanostructures as efficient catalysts for electro-chemical hydrogen evolution reaction (HER) in acidic and alkaline media. Journal of Materials Chemistry A, 8(3), 1403–1416.

Kang, M., Lin, C., Yang, H., Guo, Y., Liu, L., Xue, T., Liu, Y., Gong, Y., Zhao, Z., & Zhai, T. (2021). Proximity enhanced hydrogen evolution reactivity of substitutional doped monolayer WS_2. ACS Applied Materials & Interfaces, 13(16), 19406–19413.

Kumar, A., & Ahluwalia, P. K. (2012). Electronic structure of transition metal dichalcogenides monolayers 1H-MX_2 (M = Mo, W; X = S, Se, Te) from ab-initio theory: New direct band gap semiconductors. The European Physical Journal B, 85, 186. https://doi.org/10.1140/epjb/e2012-30070-x

Lin, Y., Dumcenco, D. O., Komsa, H.-P., Niimi, Y., Krasheninnikov, A. V., Huang, Y.-S., & Suenaga, K. (2014). Properties of individual dopant atoms in single-layer MoS_2: Atomic structure, migration, and enhanced reactivity. Advanced Materials, 26(18), 2857.

Luo, J., & Liang, C. (2024). Rhenium in heterogeneous catalysis: A rising star for hydrogenation reactions. ACS Catalysis, 14(9), 7032–7049.

Meng, H., Zhang, W., Ma, Z., Zhang, F., Tang, B., Li, J., & Wang, X. (2018). Self-supported ternary Ni–S–Se nanorod arrays as highly active electrocatalyst for hydrogen generation in both acidic and basic media: Experimental investigation and DFT calculation. ACS Applied Materials & Interfaces, 10(3), 2430–2437. https://doi.org/10.1021/acsami.7b14506

Nørskov, J. K., Bligaard, T., Logadottir, A., Kitchin, J., Chen, J. G., Pandelov, S., & Stimming, U. (2005). Trends in the exchange current for hydrogen evolution. Journal of the Electrochemical Society, 152(3), J23–J26. https://doi.org/10.1149/1.1856988

Ogunkunle, S. A., Bouzid, A., Hinsch, J. J., Allen, O. J., White, J. J., Bernard, S., Wu, Z., Zhu, Y., & Wang, Y. (2024). Defect engineering of 1T′ MX_2 (M = Mo, W and X = S, Se) transition metal dichalcogenide-based electrocatalyst for alkaline hydrogen evolution reaction. Journal of Physics: Condensed Matter, 36(14), 145002. https://doi.org/10.1088/1361-648x/ad19a4

Perdew, J.P., Burke K. & Ernzerhof M. (1996). Generalized gradient approximation made simple. Physical Review Letter,

77, 3865–3868. https://doi.org/10.1103/PhysRevLett.77.3865

Sarma, P. V., Vineesh, T. V., Kumar, R., Sreepal, V., Prasannachandran, R., Singh, A. K., & Shaijumon, M. M. (2020). Nanostructured tungsten oxysulfide as an efficient electrocatalyst for hydrogen evolution reaction. ACS Catalysis, 10(11), 6753–6762.

Schutte, W. J., De Boer, J. L., & Jellinek, F. (1987). Crystal structures of tungsten disulfide and diselenide. Journal of Solid State Chemistry, 70(2), 207–209. https://doi.org/10.1016/0022-4596(87)90057-0

Sigiro, M., Huang, Y. S., Ho, C. H., Lin, Y. C., & Suenaga, K. (2015). Influence of rhenium on the structural and optical properties of molybdenum disulfide. Japanese Journal of Applied Physics, 54, 04DH05.

Stamenkovic, V. R., Strmcnik, D., Lopes, P. P., & Markovic, N. M. (2017). Energy and fuels from electrochemical interfaces. Nature Materials, 16(1), 57–69. https://doi.org/10.1038/nmat4738

Sukanya, R., da Silva Alves, D. C., & Breslin, C. B. (2022). Review—recent developments in the applications of 2D transition metal dichalcogenides as electrocatalysts in the generation of hydrogen for renewable energy conversion. Journal of the Electrochemical Society, 169(6), 064504. https://doi.org/10.1149/1945-7111/ac7172

Sun, L., Gao, M., Jing, Z., Cheng, Z., Zheng, D., Xu, H., Zhou, Q., & Lin, J. (2022). 1T-Phase enriched P doped WS_2 nanosphere for highly efficient electrochemical hydrogen evolution reaction. Chemical Engineering Journal, 429, 132187.

Tonndorf, P., Schmidt, R., Böttger, P., Zhang, X., Börner, J., Liebig, A., Albrecht, M., Kloc, C., Gordan, O., & Zahn, D. R. (2013). Photoluminescence emission and Raman response of monolayer MoS_2, $MoSe_2$, and WSe_2. Optics Express, 21(4), 4908–4916.

Vikraman, D., Hussain, S., Patil, S. A., Truong, L., Arbab, A. A., Jeong, S. H., Chun, S.-H., Jung, J., & Kim, H.-S. (2021). Engineering $MoSe_2/WS_2$ hybrids to replace the scarce platinum electrode for hydrogen evolution reactions and dye-sensitized solar cells. ACS Applied Materials & Interfaces, 13(4), 5061.

Vuong, V. T., Nguyen, T. H., & Do, V. T. (2018). Charge-induced electromechanical actuation of Mo- and W-dichalcogenide monolayers. RSC Advances, 8(68), 38667.

Wang, F., Niu, S., Liang, X., Wang, G., & Chen, M. (2022). Phosphorus incorporation activates the basal plane of tungsten disulfide for efficient hydrogen evolution catalysis. Nano Research, 15(4), 2855–2861.

Wang, H., Xu, Z., Zhang, Z., Hu, S., Ma, M., Zhang, Z., Zhou, W., & Liu, H. (2020). Addressable surface engineering for N-doped WS2 nanosheet arrays with abundant active sites and the optimal local electronic structure for enhanced hydrogen evolution reaction. Nanoscale, 12(41), 22541–22550.

Woo, S. H., Yadgarov, L., Rosentsveig, R., Park, Y., Song, D., Tenne, R., & Hong, S. Y. (2015). Fullerene-like Re-doped MoS_2 nanoparticles as an intercalation host with fast kinetics for sodium ion batteries. Israel Journal of Chemistry, 55(5–6), 599–603.

Ye, S., Ding, C., Chen, R., Fan, F., Fu, P., Yin, H., Wang, X., Wang, Z., Du, P., & Li, C. (2018). Mimicking the key functions of photosystem II in artificial photosynthesis for photoelectrocatalytic water splitting. Journal of the American Chemical Society, 140(9), 3250–3256.

Zhang, K., Guo, Y., Ji, Q., Lu, A.-Y., Su, C., Wang, H., Puretzky, A. A., Geohegan, D. B., Qian, X., Fang, S., Kaxiras, E., Kong, J., & Huang, S. (2020). Enhancement of van der Waals interlayer coupling through polar Janus MoSSe. Journal of the American Chemical Society, 142(41), 17499–17507. https://doi.org/10.1021/jacs.0c07051

Zhang, W., Liu, X., Liu, T., Chen, T., Shen, X., Ding, T., Cao, L., Wang, L., Luo, Q., & Yao, T. (2021). In situ investigation on doping effect in Co-doped tungsten diselenide nanosheets for hydrogen evolution reaction. The Journal of Physical Chemistry C, 125(11), 6229–6236.

Zhu, J., Hu, L., Zhao, P., Lee, L. Y. S., & Wong, K. Y. (2020). Recent advances in electrocatalytic hydrogen evolution using nanoparticles. Chemical Reviews, 120(2), 851–918. https://doi.org/10.1021/acs.chemrev.9b00248